



**HAL**  
open science

## Sensitivity of simulated light interception and tree transpiration to the level of detail of 3D tree reconstructions

Elena Bournez, Tania Landes, Georges Najjar, Pierre Kastendeuch, Jérôme Ngao, M. Saudreau

### ► To cite this version:

Elena Bournez, Tania Landes, Georges Najjar, Pierre Kastendeuch, Jérôme Ngao, et al.. Sensitivity of simulated light interception and tree transpiration to the level of detail of 3D tree reconstructions. *Urban Forestry & Urban Greening*, 2019, 38, pp.1-10. 10.1016/j.ufug.2018.10.016 . hal-02342522

**HAL Id: hal-02342522**

**<https://hal.science/hal-02342522>**

Submitted on 31 Oct 2019

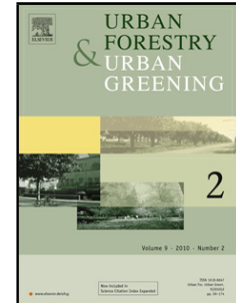
**HAL** is a multi-disciplinary open access archive for the deposit and dissemination of scientific research documents, whether they are published or not. The documents may come from teaching and research institutions in France or abroad, or from public or private research centers.

L'archive ouverte pluridisciplinaire **HAL**, est destinée au dépôt et à la diffusion de documents scientifiques de niveau recherche, publiés ou non, émanant des établissements d'enseignement et de recherche français ou étrangers, des laboratoires publics ou privés.

## Accepted Manuscript

Title: Sensitivity of simulated light interception and tree transpiration to the level of detail of 3D tree reconstructions

Authors: Elena Bournez, Tania Landes, Georges Najjar, Pierre Kastendeuch, Jérôme Ngao, Marc Saudreau



PII: S1618-8667(17)30659-3  
DOI: <https://doi.org/10.1016/j.ufug.2018.10.016>  
Reference: UFUG 26239

To appear in:

Received date: 26 October 2017  
Revised date: 15 October 2018  
Accepted date: 30 October 2018

Please cite this article as: Bournez E, Landes T, Najjar G, Kastendeuch P, Ngao J, Saudreau M, Sensitivity of simulated light interception and tree transpiration to the level of detail of 3D tree reconstructions, *Urban Forestry and amp; Urban Greening* (2018), <https://doi.org/10.1016/j.ufug.2018.10.016>

This is a PDF file of an unedited manuscript that has been accepted for publication. As a service to our customers we are providing this early version of the manuscript. The manuscript will undergo copyediting, typesetting, and review of the resulting proof before it is published in its final form. Please note that during the production process errors may be discovered which could affect the content, and all legal disclaimers that apply to the journal pertain.

## MANUSCRIPT

**Sensitivity of simulated light interception and tree transpiration to the level of detail of 3D tree reconstructions**

Elena Bournez<sup>1,\*</sup>, Tania Landes<sup>1</sup>, Georges Najjar<sup>1</sup>, Pierre Kastendeuch<sup>1</sup>, Jérôme Ngao<sup>2</sup>, Marc Saudreau<sup>2</sup>

<sup>1</sup> ICube Laboratory, UMR 7357, University of Strasbourg, CNRS, INSA, Strasbourg, France

<sup>2</sup> Université Clermont Auvergne, INRA, PIAF, 63000 Clermont-Ferrand, France

**Corresponding author:** Elena Bournez<sup>\*</sup>,

Mailing address: INSA Strasbourg, 24 boulevard de la Victoire, 67000 Strasbourg, France,

Tel.: +33 (0)3 88 14 47 33

E-mail: [elena.bournez@insa-strasbourg.fr](mailto:elena.bournez@insa-strasbourg.fr)

**HIGHLIGHTS**

- 3D reconstruction of trees can be performed using terrestrial laser scanner data.
- The ideal level of detail can be validated thanks to a reference mock-up.
- The RATP model can simulate tree transpiration rates from 3D tree mock-ups.
- Promising results can be obtained with two different tree mock-ups.
- Three main characteristics appear essential for accurate transpiration simulation.

**Abstract**

The aim of this paper is to investigate the minimal level of detail of the tree geometry reconstruction required to enable an accurate estimate of the evaporative cooling effect of an individual tree.

The Functional Structural Plant Modeling approach, which links the 3D tree structure to its functioning, is used to investigate the impact of the level of detail of a tree reconstruction on its simulated transpiration. Based on terrestrial laser scanning point cloud data of a nine-meter-high silver linden tree (*Tilia tomentosa* Moench), several methods of reconstruction of its crown were considered. They can be divided into three groups: (i) tree branching structure reconstructions where leafy shoots are reconstructed; (ii) envelope reconstructions such as 3D convex/concave envelopes; and (iii) voxel reconstructions where leaves are uniformly distributed within the given volume. Based on these methods, several mock-ups of resolved tree crowns from low to high level of details were created. The cooling performance of each tree mock-up was compared by simulating its transpiration rate with a validated 3D ecophysiological model based on the turbid medium approach.

The resulting mock-ups differ in several characteristics related to tree metrics and light interception: volume, projected leaf area, leaf area index, leaf area density, leaf clumping and silhouette-to-total area ratio. An inter-comparison of the transpiration rates provided by these mock-ups shows that tree branching structure reconstruction methods perform better than envelope computation methods and that these differences are related to the light interception property of the reconstructed trees.

This study provides guidelines to determine which structural characteristics of tree crowns must be measured and taken into account in order to carry out accurate estimates of the transpiration rates of individual trees.

**Key words:** Branching skeleton; Envelope; Light interception; Transpiration; Urban tree; Voxels.

## 1. INTRODUCTION

### *1.1. Trees in cities to cool the urban atmosphere*

Cities are mainly composed of mineral materials (ground, buildings) and are very sensitive to climatic heat waves through the “urban heat island” effect (Oke, 1982). Among the adaptation strategies of cities to climate change, “greening”, i.e., reintroducing vegetation and, in particular, trees within cities, is a promising way (Rosenzweig et al., 2009). Through transpiration and shading, trees have a significant impact on the heat balance of the surrounding atmosphere (Peters et al., 2011) and may reduce air temperature by several degrees (Bowler et al., 2010). This positive impact is strengthened by ecosystem services that trees could provide to city dwellers: pollution clean-up (air and soil), carbon sequestration, social well-being and biodiversity (Mullaney et al., 2015).

### *1.2. Integrating trees into urban climate models*

To mitigate the expected increase in heat waves frequency and intensity resulting from global climate change (IPCC, 2007) and to provide guidelines for urban planners, specific tree modules are added to urban climate models to simulate the interactions between trees and urban climate (Redon et al., 2017). The ability of trees to intercept light is strongly linked to their geometry, which determines the surface area and the intensity of the shade and, indirectly, their transpiration rate (Ross, 1981). Therefore, the integration of trees into urban climate models raises the question about the minimal level of detail (LOD) required for tree geometry reconstruction that would allow an accurate estimate of light interception and, consequently, of the shading and evaporative cooling processes. Trees are rarely integrated into urban climate models at this time. The reconstruction is usually very coarse with simple geometric shapes that

do not permit the good simulation of tree radiation properties and functions (Redon et al., 2017). A better reconstruction of trees is therefore needed that may require fine-scale measurements of tree geometry. However, in view of the large number of urban trees and their diversity in terms of structure, which changes during the growing season, it is necessary to find a trade-off between the LOD of tree reconstruction, and the relevancy of the simulated processes. Identifying the most relevant tree shape characteristics that drive tree functions is therefore crucial.

### 1.3. *Tree crown characteristics*

Light interception and transmission by tree canopies has been studied for many years, both experimentally and theoretically (Chartier, 1966; Monsi and Saeki, 1953; Nilson, 1971; Ross, 1981). More recently, these studies have become numerical with 3D virtual trees based on functional structural plant models (Da Silva et al., 2012; Green, 1993; Sinoquet et al., 2001; Wang and Jarvis, 1990). All of these studies provide some useful tree canopy characteristics that directly impact light interception and transmission. Results differ between the continuous canopies that can be observed in parks and forest stands, and individual trees that can be observed in cities, such as those along the streets. For continuous canopies and for a given leaf angle distribution, the Leaf Area Index ( $LAI = TLA/PLA$ , where  $TLA$  ( $m^2$ ) is the Total Leaf Area and  $PLA$  ( $m^2$ ) is the ground Projected Leaf Area) is the main characteristic that can be linked to the amount of light intercepted by the entire foliage (Breda, 2003). Moreover, the LAI is generally used to predict transpiration and photosynthetic rates (Caldwell et al., 1986). For individual trees, the light can be intercepted from many directions. Consequently, other characteristics related to the 3D geometry of the tree crown are important. A recent study by Sinoquet et al. (2007) shows that the Projected Envelope Area ( $PEA - m^2$ ), the clumping factor ( $\mu$ ), the  $TLA$  and the Leaf Area Density ( $LAD - m^2/m^3$ ) are all important characteristics for estimating light interception by an isolated tree crown.

#### 1.4. 3D tree reconstruction

Tree functions are known to depend on the spatial distribution of the leaf surface. An efficient tree reconstruction method should therefore be able to reproduce the right leaf surface area and its distribution within a canopy as closely as possible. From a plant-atmosphere modeling point of view, a tree can be viewed as a 2D surface that shades a fraction of the ground. Moreover, this surface can be capable of releasing water vapor at a given rate that correlates with its LAI (Noilhan and Planton, 1989). A tree can also be considered as a 3D object with a reconstruction of the tree crown that can vary from simple 3D geometrical shapes such as spheres, cubes and pyramids (Da Silva et al., 2012), to a fine 3D reconstruction of the branching structure and leaves (Boudon et al., 2014). This kind of reconstruction requires the use of specific 3D acquisition techniques. In the literature, three main techniques are used for acquiring 3D tree point clouds, i.e., a set of vertices in a three-dimensional coordinate system: manual electromagnetic digitizing, photogrammetric techniques and laser scanning techniques. The first technique is based on the measurement of the 3D location of a pointer that enables to retrieve 3D coordinates of specific points of the tree components (shoots, fruits, leaves), as explained in (Sinoquet and Rivet, 1997). This technique is largely used in tree structure measurement especially for acquiring the tree topology (i.e. branching patterns) (Sellier and Fourcaud, 2005) or estimating the leaf surface distribution (Sonohat et al., 2006). Although this technique is adapted for accurate reconstructions, the acquisition step remains manual and tedious. Photogrammetric and laser scanning techniques are faster and require less manual interventions than the first one and do not require any contact with the object under study. Based on terrestrial photographs, a tree point cloud can be generated by dense image matching from which global tree metrics such as the tree crown volume, height and diameter or 3D mesh reconstructions can be obtained (Morgenroth and Gomez, 2014; Phattaralerphong and Sinoquet, 2005). Even small tree structures can be detected with terrestrial photographs (Miller et al.,

2015). This technique is easily operated and is a very cheap alternative to laser scanning (Miller et al., 2015). A drawback of the photogrammetric technique is that a huge number of points of view is required to obtain enough data for the reconstruction of only one tree. Finally, the terrestrial laser scanning technique seems to be the most adequate solution since Terrestrial Laser Scanning (TLS) allows a fast and accurate acquisition of dense point clouds (van Leeuwen and Nieuwenhuis, 2010). Moreover, a dense point cloud can now be associated with efficient reconstruction methods of the crown branching structure (Boudon et al., 2014; Mei et al., 2017) and foliage characteristics (Béland et al., 2011).

### 1.5. Scope of the paper

This study proposes an in-depth examination of the impact of the level of detail of tree crown reconstruction on the simulated evaporative cooling effect of an individual tree. For this purpose, several leafy mock-ups of the crown of a nine-meter-high silver linden tree (*Tilia tomentosa* Moench) with different levels of detail were made using TLS data. The cooling performance of each tree mock-up was estimated by simulating its transpiration rate with the RATP (Radiation Absorption, Transpiration and Photosynthesis) model, a validated 3D ecophysiological model based on the turbid medium approach (Sinoquet et al., 2001). The performance of each mock-up in terms of transpiration was compared to a reference mock-up in order to determine the required level of detail that should be reached to properly simulate the tree transpiration. The differences in transpiration rates are linked to the differences in some tree crown characteristics taken from the literature that were considered to drive light interception of individual tree canopies. In addition to determining the best reconstruction strategy to be adopted, this study highlights the relevant characteristics to be measured in the field to ensure a good estimate of the tree transpiration rate.

In the following section, the different processes leading to the simulation of the transpiration rate of a silver linden tree based on several tree mock-ups are discussed. In

Section 3, the impact of the LOD on tree crown characteristics and transpiration is studied on the basis of the results obtained for each mock-up. The relationships between differences in transpiration rates and tree characteristics are also discussed. Section 4 is devoted to a discussion on the benefits and drawbacks of the tree reconstruction methods according to the simulated transpiration rates, and Section 5 presents the conclusion with perspectives for the future.

## 2. MATERIALS AND METHODS

### *2.1. Tree point cloud acquisition*

The tree under study is a silver linden tree pruned in a short head shape (Clair-Maczulajtyś and Bory, 1988), i.e., all vegetative shoots are removed at branch extremities. Fig. 1a shows the silver linden tree under study in winter (at the right) and in summer (at the left). The extremity of a branch and its vegetative shoots are known as “short head”. All of the reconstructions carried out in this study are based on two distinct point clouds (Fig. 1c) acquired during field measurements with a TLS sensor (Faro Focus 3D X330) (Landes et al., 2014). All point clouds cover the same tree but were captured at different times: (i) the tree with leaves at the end of the summer (Fig. 1c at the left) and (ii) in winter when all the leaves have fallen and only annual shoots can be seen (Fig. 1c at the right). As shown in Fig. 1b, at least four stations are realized around the tree under study in order to acquire a point cloud covering the whole tree. The point spacing has been set to 6 mm at 10 m range for the tree with leaves and to 3 mm at 10 m range for the leafless tree with shoots.

*(Place of Fig. 1 without color in print)*

### *2.2. Tree crown reconstruction methods*

To simulate linden tree transpiration, two different tree reconstructions were made, one with the aim of obtaining accurate simulations at the tree scale and the other one in view of

being able to simulate the transpiration rates of several trees simultaneously. For this purpose, a detailed mock-up with leaves on shoots and a coarse mock-up consisting of an envelope with leaves uniformly distributed inside, respectively, were created. Mock-ups with intermediary LODs were then made in order to validate or not some assumptions on the leaf distribution in the crown. As depicted below, each point cloud is useful to create mock-ups and helps to produce specific LODs.

Reconstructed 3D mock-ups are classified into three groups according to the method of reconstruction used, as illustrated in Fig. 2: Group I is composed of tree branching structure reconstructions, Group II of envelope reconstructions such as 3D convex/concave envelopes, and Group III of voxel reconstructions. In the end, a total of 15 mock-ups of the same tree with different LODs was produced. The different codes developed to reconstruct the mock-ups were written in Matlab software (MathWorks). Also the AutoCAD software (Autodesk) has been used for manual reconstruction.

*(Place of Fig. 2 without color in print)*

The first group of reconstruction methods provides the most detailed and faithful to reality mock-ups, as it is characterized by a leaf distribution around the shoots. The assessment of two existing reconstruction methods based on cylinder adjustments (Hackenberg et al., 2015) and skeletonization (Landes et al., 2014; Boudon et al., 2014) led us to choose the latter method for shoot reconstruction. A skeleton is considered as a compact and efficient representation of a solid shape, faithfully representing the geometry and topology shapes (Jiang et al., 2013). The methods implemented therefore consist in reconstructing shoots using skeletonization methods based on leafless tree point clouds (Bournez et al., 2016). Then, for all these methods, leaves are reconstructed on each reconstructed shoot using allometric statistics. These statistics connect leaf surface area and number of leaves borne by a shoot to the shoot length. It is therefore necessary to sample shoots for each tree or tree species studied (Sonohat et al., 2006).

A leafy point cloud could also be used to retrieve the 3D branching structure and the position of leaves (Xu et al., 2007). Unfortunately, the problem is unsolvable for tree crowns with dense foliage, such as the linden tree studied. Seven mock-ups compose this first group. Their branching structures are depicted in the first row of Fig. 2. A reference mock-up called LOD ref<sub>(l)</sub> was performed by manual digitalization of the shoots bearing leaves inside the point cloud in the software AutoCAD. LOD ref<sub>(l)</sub> therefore provides a true reconstruction of the shoots with their real position, number (919 shoots), length (958.9 m) and curvature. The skeleton of LOD 4<sub>(l)</sub> is very close to the reference skeleton but with some simplifications according to the number (1326 shoots) and the length (925.5 m) of reconstructed shoots. The automatic process leads to reconstruct +44% more branches compared to the reference. However, the total length of shoots compared to the reference is only about -3%. These differences are due to the method of reconstruction used for obtaining LOD 4<sub>(l)</sub>. For this mock-up, the automatic skeletonization algorithm of Xu et al. (2007), also integrated into the PlantScan3D tool (Boudon et al., 2014), is used to reconstruct shoots. In Bournez et al. (2017), the evaluation of the accuracy of the reconstructed shoots, which led to the choice of PlantScan3D for the reconstruction, is presented. Concerning LOD 2<sub>(l)</sub>, not only the number (1092, i.e. +19% compared to the reference) and length (851.0 m, i.e. -11% compared to the reference) of shoots are generalized but their position as well. Finally, in addition to the previous characteristics, LOD 1<sub>(l)</sub> considers straight shoots instead of curved shoots. The number of reconstructed shoots is therefore equal to the LOD 2<sub>(l)</sub>, and the total length of shoots is reduced to 822.2 (-3% and -14%, compared to the LOD 2<sub>(l)</sub> and the reference, respectively). The semi-automatic methods used for generating the two last mock-ups were presented in Bournez et al. (2016). Shoots of one reconstructed short head (by manual digitalizing) was duplicated as many times as there are branches, at their extremities. As illustrated in Fig. 2, the consequences of all of these generalizations are that shoot characteristics (length, position, etc.)

are different from one mock-up to another, even for a same short head. Accordingly, the TLA of each mock-up varies as well. In order to exclude the effect of TLA variation in the analyses, three duplicates of LOD 4<sub>(I)</sub>, LOD 2<sub>(I)</sub> and LOD 1<sub>(I)</sub>, referred to as LOD 4-TLAref<sub>(I)</sub>, LOD 2-TLAref<sub>(I)</sub> and LOD 1-TLAref<sub>(I)</sub>, were produced. These new mock-ups for Group I make it possible to have the same TLA as the reference mock-up.

The second group of reconstruction methods uses a simpler methodology than the previous group with an envelope-based approach. Firstly, the process involves the creation of a convex or a concave envelope that drapes the point cloud as closely as possible (Zhu et al., 2008). Envelopes were reconstructed with the alpha shape function in Matlab. Then leaves are uniformly spaced in the envelope. Based on TLS data, some methods make it possible to determine TLA and LAD per tree (Kong et al., 2016; Kumakura et al., 2010; Oshio et al., 2015). However, in this study, the choice was made to simplify the reconstruction process with a uniform leaf distribution in the envelope. As illustrated in the second row of Fig. 2, this second group contains four mock-ups referred to as LOD 0.8<sub>(II)</sub>, LOD 0.6<sub>(II)</sub>, LOD 0.5<sub>(II)</sub> and LOD 0<sub>(II)</sub>. The particularity of these mock-ups is the use of different types of envelopes for characterizing the tree crown geometry. The tree reconstruction is coarser from LOD 0.8<sub>(II)</sub> to LOD 0<sub>(II)</sub>. In LOD 0.8<sub>(II)</sub>, convex envelopes around the shoots on short heads, available on the leafless point cloud were reconstructed. There are as many reconstructed envelopes as there are branch extremities. The same leaf area as the reference case was uniformly distributed in each envelope. Regarding the creation of the other mock-ups, the leafy point cloud is used for the envelope computations. Both LOD 0.6<sub>(II)</sub> and LOD 0.5<sub>(II)</sub> leaves are located in an envelope that encompasses the entire tree crown (dark green envelope in Fig. 2) except in a central part that is considered to be free from leaves (light green envelope in Fig. 2). Based on the branch extremities, this central part was removed from the envelope. The main difference between LOD 0.6<sub>(II)</sub> and LOD 0.5<sub>(II)</sub> is the type of envelope (concave for LOD 0.6<sub>(II)</sub> and convex for

LOD 0.5<sub>(II)</sub>). The concave envelope allows a more reliable and realistic reconstruction of the crown shape than the convex envelope. Finally, in LOD 0<sub>(II)</sub>, leaves are positioned in the whole convex envelope of the crown, without taking a central hole in the crown into account.

Concerning the third group of reconstruction methods, a voxel-based approach was used to create four mock-ups: LOD 0.5-Vox20<sub>(III)</sub>, LOD 0-Vox20<sub>(III)</sub>, LOD 0.5-Vox50<sub>(III)</sub> and LOD 0-Vox50<sub>(III)</sub>. The point cloud of the leafy tree crown is discretized into several voxels according to a given voxel size (width = length): 20 cm and 50 cm. Obviously, the accuracy of the created mock-ups depends on the voxel size used. The leaf area is uniformly distributed in each voxel. The third row of [Fig. 2](#) presents LOD 0.5-Vox50<sub>(III)</sub> and LOD 0-Vox50<sub>(III)</sub> created with a voxel size of 50 cm with a volume with or without leaves, respectively, as in the second group of mock-ups.

For the 15 mock-ups, the leaf angle distributions (inclination and azimuth) were considered to be the same. Moreover, the TLA of LOD ref<sub>(I)</sub> is used for the reconstruction of all the mock-ups, except for LOD 4<sub>(I)</sub>, LOD 2<sub>(I)</sub> and LOD 1<sub>(I)</sub>, in order to exclude the effect of TLA variation in the analyses. The created mock-ups therefore only differ according to the crown volumes and regarding the way the leaves are distributed inside the crown.

### 2.3. Tree crown characteristics

In order to analyze the impact of the different LODs on the foliage properties in terms of their spatial distribution and their ability to intercept light, several characteristics were computed and are presented in Table 1. Based on a discretization of each mock-up into cubic voxels of 20 cm in size, as explained in Subsection 2.4, the PLA, the volume and the TLA were retrieved. On the basis of these primary characteristics, the LAI and the LAD were also computed. For light interception properties, two characteristics were computed according to the methodology of Sinoquet et al. (2007): the  $\mu$  and the diffuse Silhouette-to-Total Area Ratio (STAR). The  $\mu$  accounts for the effect of non-random and non-uniform distribution of LAD in

a crown volume. Deviation from random dispersion ( $\mu = 1$ ) usually occurs in actual tree canopies that generally present a leaf clumping ( $\mu < 1$ ). STAR is a sky-integrated value that characterizes the overall interception properties of the trees:

$$STAR = \sum_{i=1}^{46} \omega_{\Omega} STAR_{\Omega} \quad (1)$$

Where  $\omega_{\Omega}$  and  $STAR_{\Omega}$  are the weight and the STAR value, respectively, associated with the direction  $\Omega$ .  $\omega_{\Omega}$  are computed according to the Standard OverCast sky radiance distribution, which was discretized into 46 solid angle sectors of equal area (Den Dulk, 1989).

#### 2.4. Tree crown transpiration rate

The tree crown transpiration was estimated with the RATP model. A complete description and assessment of the model can be found in Sinoquet et al. (2001). Its main characteristics are summarized below. It was designed to simulate the spatial distribution of radiation and leaf-gas exchanges within vegetation canopies as a function of canopy geometry, microclimate within the canopy and physical and physiological leaf properties. It is based on a turbid medium analogy for radiation transfers in the canopy, described as a set of voxels. The radiative transfer sub-model is aimed at (i) sending beams into the canopy according to the directional distribution of incident radiation, by taking into account for the sun direction and the distribution of incident radiation into direct and diffuse radiation; radiance distribution for diffuse radiation is assumed to obey the standard overcast sky (Moon & Spencer 1942); (ii) identifying the 3D sequence of cells crossed by any light beam; (iii) determining the beam path length within each crossed cell; and (iv) applying Beer's law to calculate beam extinction within each crossed voxel (Sinoquet et al. 2001). Radiation sources are the sky, including direct and diffuse (i.e. scattered by clouds and atmospheric gases) fraction of incident radiation, as well as foliage components and soil surface which scatter a fraction of radiation they intercept. The spatial distribution of leaf temperature is estimated by closing the energy balance equation between incoming and outgoing fluxes. The local transpiration rate of the leaves within a voxel

is driven by the physiological response of the plant (stomatal conductance) and the evaporative demand (Monteith and Unsworth, 1990). In the RATP model, the stomatal conductance is controlled by the microclimate surrounding the leaves (intercepted PAR, CO<sub>2</sub> and VPD) and the leaf temperature according to the Jarvis model (Jarvis, 1976). The input data for simulating the transpiration of one tree are: (i) a grid of 20-cm voxels dimensioned according to the tree crown size; (ii) a set of functional parameters; and (iii) meteorological data. A more detailed description of all the parameters used in RATP is not shown for the sake of brevity, but whole parameters are based on field measurements (Bournez et al., 2016). For instance, forcing meteorological variables were taken from a subset of meteorological data measured in the city of Strasbourg where the silver linden tree studied is located (Najjar et al., 2015). The dataset is composed of 19 days in the summer of 2014. The time step is one hour and was chosen to ensure a high variability in the simulated transpiration rate of LOD ref<sub>(1)</sub>. In practice, each mock-up, reconstructed with individual leaves as described above, is immersed in a grid composed of cubic voxels with 20-cm-long sides. The voxels are then filled with a certain quantity of leaf area determined according to the number of leaves they contain. For each meteorological time step, the tree transpiration rate of a tree mock-up is finally computed by summing the transpiration rate of all of the voxels.

### 2.5. Statistical analyses

All the statistical analyses carried out in this article were performed with STATGRAPHICS Centurion XVI software (StatPoint Technologies, Inc.).

An analysis of variance (ANOVA) followed by a Fisher's LSD test were performed to compare the mean foliage characteristics of the three groups of reconstruction methods. In each group, four mock-ups ( $n = 4$ ) were used in order to have the same number of samples for each group. In the results, letters indicate the significance of homogeneous groups with the p-value level set to 0.05.

Multiple linear regression analyses were done to relate the simulated transpiration deviations of the mock-ups from the reference case to foliage characteristics. Both forward and backward methods were used and statistical models were compared in terms of adjusted coefficients of determination ( $R^2$ ) and Mean Absolute Error (MAE). In the case of simple linear regression analysis, the MAE, the Mean Square Error (MSE), the Mallow's coefficient ( $C_p$ ), the slope ( $a$ ), the intercept ( $b$ ), and the  $R^2$  of the regression fit were estimated. The significance of each simple linear regression was assessed with an F-test with a significant p-value level set to 0.05.

### 3. RESULTS

Based on the LOD of each mock-up, three comparisons were carried out in terms of: (i) the tree crown characteristics; (ii) the tree crown transpiration; and (iii) the relationship between the two.

#### 3.1. Comparison of the tree crown characteristics between LODs

Based on the same point cloud dataset, the three groups of reconstructions definitively lead to different tree crown mock-ups (Fig. 2) and related characteristic values (Table 1). This is confirmed in Fig. 3 by the statistical comparison of mean values of tree crown characteristics between the reconstruction groups. To ensure the same number of samples between groups, LOD 4-TLAref<sub>(I)</sub>, LOD 2-TLAref<sub>(I)</sub> and LOD 1-TLAref<sub>(I)</sub> were removed from this statistical analysis. Four mock-ups ( $n = 4$ ) are therefore used for each group.

*(Place of Table 1 and Fig. 3 without color in print)*

As depicted in Fig. 3, trees reconstructed from branching structure reconstructions (Group I) present smaller crown volumes and PLAs than trees with crown shapes estimated by envelopes (Group II) or voxels (Group III). The order is reversed when considering the LAD. Referring to Table 1, this result sounds logical since the TLA is nearly constant between mock-

ups (about 215.2 m<sup>2</sup> for the Group I and 233.4 m<sup>2</sup> for the Group II and III), whereas the volume of the crowns decreases (about 34.4 m<sup>3</sup>, 68.5 m<sup>3</sup> and 73.3 m<sup>3</sup> for the Group I, the Group II and the Group III, respectively). On the contrary, the use of envelopes or voxels does not lead to significant differences in any of the characteristics, except for the clumping factor (about 0.73 and 0.85 for the Group II and the Group III, respectively). Even if the LAI and the STAR values are different for all groups, they only differ significantly between the voxel reconstructions and the branching structure reconstructions. The highest LAI (about 10.8 m<sup>2</sup>/m<sup>2</sup>) and lowest STAR (about 0.15) were obtained with the reconstructions based on the branching structure.

Although the number of samples in each reconstruction group is low, the intra-method variations of these characteristics reveal different trends according to the LOD, as indicated in Table 1. For trees reconstructed from branching structure reconstructions, the tree crown volumes, the PLA and the STAR decrease with decreasing LOD values. Inversely, the LAD and the clumping factor increase. The LAI seems to be roughly constant over the LODs. These results do not depend on the TLA since mock-ups with the same TLA values (LODs-TLAref<sub>(I)</sub>) present the same trends. The transition from curved (LOD 2<sub>(I)</sub>) to straight shoots (LOD 1<sub>(I)</sub>) does not considerably change the characteristic values compared to the changes induced by moving from LOD 4<sub>(I)</sub> to LOD 2<sub>(I)</sub> or to LOD 1<sub>(I)</sub>. For the tree crowns reconstructed from an envelope, trends are reversed, except for the clumping factor. Indeed, values of the volume, the PLA, the STAR and the clumping factor increase, and values of the LAD and LAI decrease when the LOD of the mock-ups decreases. Finally, and for the trees reconstructed with voxels, the voxel size has a greater effect on characteristic values than when taking the space without leaves in the tree crown into account (LOD 0.5<sub>(III)</sub> vs. LOD 0<sub>(III)</sub>). When the voxel size decreases the volume, the PLA, the STAR and the clumping factor decrease, whereas the LAD and the LAI increase.

### *3.2. Comparison of the tree crown transpiration rate between LODs*

To estimate the impact of the LOD on the whole tree crown transpiration rate, hourly transpiration rates of each LOD were plotted against hourly transpiration rates computed with the reference case, LOD ref<sub>(I)</sub>. As an illustration of the deviation from LOD ref<sub>(I)</sub>, the average values of hourly transpiration rates among groups compared to LOD ref<sub>(I)</sub> values are presented in Fig. 4. A linear regression with the intercept forced to zero was performed for each LOD. The slopes,  $a_T$ , of each linear regression are listed in Table 1.  $R^2$  coefficients are not indicated in Table 1 because they are all higher than 0.99. This analysis shows that the deviation from the reference case depends on the reconstruction group. As expected, the best group is the first one, based on the tree branching structure reconstruction, with an average deviation of -7% (from -13% to +2% between LODs). The third group, using the voxelization of the leafy tree point cloud, gives the worst results, with an average deviation of +30% (from +16% to +44% between LODs). The envelope reconstruction group (Group II) falls in the middle with an average deviation of +10% (from -6% to +20% between LODs).

*(Place of Fig. 4 without color in print)*

In Table 1, it can also be noted that the intra-variability of the transpiration rate is high for a given reconstruction group. It depicts the sensitivity of the tree transpiration rate to several tree crown characteristics. Table 1 shows that the transpiration rate simulated with LOD 4<sub>(I)</sub> differs from LOD 2<sub>(I)</sub> and LOD 1<sub>(I)</sub> simulations. In particular, LOD 4-TLAref<sub>(I)</sub> with the same TLA as the reference provides a very good estimate of the tree transpiration rate. In contrast, consideration of curved or straight shoots (LOD 2<sub>(I)</sub> vs. LOD 1<sub>(I)</sub>) does not change the whole tree transpiration rate. Between the tree mock-ups based on the envelope reconstruction, the transpiration rates simulated with LOD 0.5<sub>(II)</sub> and LOD 0<sub>(II)</sub> deviate more from the reference case than the transpiration rate simulated with LOD 0.8<sub>(II)</sub> and LOD 0.6<sub>(II)</sub>. Moreover, the space without leaves in the tree crown (LOD 0.5<sub>(II)</sub>) does not impact the transpiration rate since only a tiny difference is simulated compared to the crown filled with leaves (LOD 0<sub>(II)</sub>). Finally, the

voxel size (LODs-Vox50<sub>(III)</sub> vs. LODs-Vox20<sub>(III)</sub>) has a greater effect on the transpiration rate than taking the space without leaves in the inner part of the tree crown into account (LODs 0.5<sub>(III)</sub> vs. LODs 0<sub>(III)</sub>).

### 3.3. Relationship between differences in transpiration rates and tree foliage characteristics

In order to link the deviation of the simulated transpiration rates from the reference, i.e., the  $a_T$  slope, with the foliage characteristics of the different LODs, a stepwise multiple regression analysis was initially performed with structural characteristics and the  $a_T$  slope values. The best model that fits the data is a combination of the tree crown volume ( $V$ ), the  $PLA$  and the  $LAI$ :

$$a_T = 0.15708 - 0.00209307 \times V + 0.0588658 \times PLA - 0.0274783 \times LAI \quad (2)$$

with an adjusted  $R^2$  of 0.986 and a MAE of 0.0128. Both backward and forward regression methods gave the same results. However, since the  $LAI$  is directly linked to the  $PLA$  ( $LAI = TLA/PLA$ ), and since the  $PLA$  is easier to measure in the field than the  $LAI$ , the  $LAI$  was removed from the analysis. The best model was obtained with the  $V$  and the  $PLA$  only:

$$a_T = -0.349398 - 0.00209135 \times V + 0.0687618 \times PLA \quad (3)$$

with an adjusted  $R^2$  of 0.985 and a MAE of 0.0165. However, with this model, two characteristics have to be measured in the field and the matrix correlation between variables revealed high correlations between the  $PLA$  and the  $V$  (correlation coefficient = - 0.9388).

*(Place of Table 2 without color in print)*

In order to determine if the transpiration can be obtained with only one characteristic and which one is the most relevant, simple regression analyses were done for each structural and light characteristic. The adjusted  $R^2$ , MSE, MAE, Cp, a, and b of each linear regression are listed in Table 2. All linear regressions are significant (p-value <0.05). Since  $PLA$  and  $STAR$  are the main characteristics that may explain  $a_T$  values with the best  $R^2$  coefficients, the relationships between  $a_T$  and  $PLA$ , and  $a_T$  and  $STAR$  are plotted in Figs. 5 and 6, respectively.

*(Place of Fig. 5 and 6 without color in print)*

As shown by Table 2 and illustrated in Figs. 5 and 6, an increase in the whole tree transpiration rate is correlated with an increase in the ground surface area (PLA) and in the leaf surface area that intercepts the light (STAR). This observation indicates that the deviation from the transpiration rate of the reference case can be explained by the difference in the ability of light interception by the tree crown according to its LOD. Thus, mock-ups that provide trees with low STAR and PLA values, i.e., LOD<sub>S(I)</sub> and LOD 0.8<sub>(II)</sub>, lead to underestimations of the transpiration rate compared to the reference case. On the other hand, the mock-ups that provide trees with high STAR and PLA values, i.e., LODs lower than 1 (Groups II and III) except for the LOD 0.8<sub>(II)</sub>, overestimate the transpiration rate compared to the reference case. The LOD 4<sub>(I)</sub> and the LOD 4-TLaref<sub>(I)</sub> involve reverse transpiration rate in comparison with the LODs in the Group I. The same trend is observed for the LOD 0.8<sub>(II)</sub> in comparison with the LODs in the Group II. It could be explained by their characteristic differences compared to their group. The LOD 4<sub>(I)</sub> and the LOD 4-TLaref<sub>(I)</sub> have almost the same PLA than the reference but a higher STAR. These LODs involve a transpiration rate almost similar to the reference case, with an overestimation of +2% with the LOD 4<sub>(I)</sub>. Contrary to the LODs of Group II, the LOD 0.8<sub>(II)</sub> have a lower PLA and STAR than the reference case, therefore it involves a transpiration rate underestimation of -6% compared to the reference case. Among LOD 4<sub>(I)</sub> to LOD 1<sub>(I)</sub>, setting the TLA to the LOD ref<sub>(I)</sub> case leads to a decrease in the STAR values and, consequently, a decrease in the transpiration rate, whereas the PLA remains constant. Among the LODs obtained with the envelope reconstructions, LOD 0.8<sub>(II)</sub> performs the best with PLA, STAR and  $a_T$  values because they are close to the reference case values.

Based on the results presented above, a discussion of the overall study is proposed below.

#### 4. DISCUSSION

Analysis of the mock-ups created in this study has shown that the reconstruction methods proposed in Group I provide leaf surface distribution characteristics that are closer to the reference case than with the mock-ups created with the reconstruction methods of Group II and III (Fig. 3). Many theoretical studies have shown the high correlation between foliage properties and light interception ability of homogeneous or complex 3D trees (Ross, 1981; Sinoquet et al., 2007). Thus, the better light interception ability (STAR values) of trees reconstructed from the underlying branching structure (Table 1 and Fig. 6) is probably a direct consequence of the tree crown characteristics. The relationship between the tree transpiration and its crown reconstruction has not been investigated in depth. Indeed, the transpiration results from a coupling between the physiological response of the leaves and the microclimate (Campbell and Norman, 1998; Monteith and Unsworth, 1990). Consequently, the only way to investigate this relationship is to use numerical models that spatialize the leaf surface and the microclimate (Green, 1993; Saudreau et al., 2013). The use of the RATP model in this paper makes it possible to carry out such investigations. The analysis of the transpiration performance of each mock-up compared to the reference case indicated that the mock-ups of Group I involve better estimations of the transpiration (-7% deviation from the reference) than with the mock-ups of Group II and III (+10% and +30% deviation from the reference, respectively). In order to explain these differences, a regression analysis between the deviation of the simulated transpiration rate from the reference case and the tree crown characteristics was carried out to correlate the deviation of transpiration with crown characteristics. Results revealed that the tree crown volume, the PLA and the diffuse STAR are highly correlated with these deviations and, consequently, with the transpiration rate of the whole tree (Table 2). These results support the findings of the experimental work of Kong et al. (2016) on the cooling effect of urban trees. They reported that the tree crown volume and the shade (PLA) provide a good indication of the

climatic impact of the tree canopy through transpiration and shading effects. This information is therefore crucial for estimating tree functions or ecosystem services provided by trees (such as the cooling effect in urban areas) on the basis of geometrical characteristics that can be easily estimated from in-field measurements.

In view of the previous analyses, a detailed branching structure approach (Group I) should be used to create mock-ups in order to accurately simulate the tree transpiration rate compared to the reference case. Our study emphasizes that the tree mock-up that provides the best results (LOD 4<sub>(I)</sub>) is based on an automatic reconstruction of the shoots using PlantScan3D software (Boudon et al., 2014). This means that the reconstruction method of LOD 4<sub>(I)</sub> may be applied to other tree geometries and may provide satisfactory tree mock-ups. However, this reconstruction method presents some drawbacks and may have to be applied according to a given methodology. For instance, leafless trees rather than leafy trees have to be considered due to the occlusion of the branching structure by leaves and the high LAD. Moreover, some branches may not support the leaves. In that case, a methodology has to be developed to reconstruct only the shoots that might bear leaves. Finally, information about leaf area distribution and leaf angle distribution on shoots has to be provided in order to reconstruct 3D mock-ups of trees with leaves.

This is the reason why reconstruction methods with envelopes (Group II) and voxels (Group III) have to be considered and analyzed, even if our results show that they do not perform as well as the branching structure approach (Group I). Indeed, they are the only methods available for tree crowns scanned with low TLS acquisition accuracy. It occurs when trees have high LADs or when a large number of trees have to be scanned over a given timeframe. The use of a concave envelope (+7% transpiration deviation from the reference with LOD 0.6<sub>(II)</sub>) rather than a convex envelope (+19% deviation with LOD 0.5<sub>(II)</sub>) or the use of small voxels (about +18% deviation with LODs-Vox20<sub>(III)</sub>) rather than large voxels (about

+43% deviation with LODs-Vox50<sub>(III)</sub>) lead to better results for all of the characteristics because they favor reconstructed crown shapes that more closely follow the tortuosity of the real tree crown. This is consistent with previous studies on volume estimation by voxels (Béland et al., 2014; Sinoquet et al., 2005). However, since a tree crown has a fractal geometry, the sensitivity of the volume to the choice of the size of the voxel may be more or less pronounced. This requires an a priori choice of the relevant voxel size that is difficult to determine (Da Silva et al., 2008; Sinoquet et al., 2005). Among mock-ups based on envelope reconstruction analyzed in this study, the use of one envelope per short head (LOD 0.8<sub>(II)</sub>) is efficient since this method favors a tree crown that is close to the reference case (-6% of transpiration deviation from the reference). However, it seems difficult to extract these leafy short heads without using the reconstructed branching structure (Da Silva et al., 2008).

The previous analyses lead us to conclude that the deviations of transpiration are actually linked to the type of tree reconstruction approach implemented. The methods used in Group I can be linked to a first approach based on a bottom-up methodology where the leaf surface distribution emerges from the reconstruction of the branching structure that bears leaves. In contrast, the methods used in Group II and III can be associated with a second approach that is instead based on a top-down concept where the larger scale (i.e., the simple crown reconstruction) is first resolved and local information about leaves is added in a second step. Information about leaves can be inferred from a TLS dataset. The bottom-up approach seems to allow the reconstruction of more detailed characteristics in the tree crown than the top-down approach.

Not one tree but several trees should be considered when determining the energy balance of a district with an urban climate model. As previously mentioned and according to the limitations of bottom-up approaches, a top-down approach for reconstructing trees would be preferable in this situation. However, and as highlighted in this study, the top-down approach

leads to an overestimation from +7% to +44% (without considering the exception of the LOD 0.8<sub>(II)</sub>) of the cooling effect of one tree, which may have a significant impact on the energy balance when several trees are considered. This is the reason why the reconstruction methods of top-down approaches, as proposed with the ones in Group II and III, could perhaps be improved. The focus of this study was not to perform a sensitivity analysis of all the input characteristics related to the tree reconstruction on the simulated transpiration, which is why, at this stage and for all the mock-ups of Group II and III, the leafy tree point cloud was not used to infer structural characteristics such as TLA, LAD and LAI (Béland et al., 2011; Kong et al., 2016), and the leaf surface area was uniformly distributed inside the reconstructed crown volume. However, a LOD efficiency of less than 1 (Group II and III) in terms of their ability to reproduce structural characteristics and functional traits might be largely improved if information about leaf distribution within the tree crown is added.

## 5. CONCLUSION

This paper presents the potential of different methods of tree crown reconstruction according to a reference method, for determining the transpiration rates of isolated trees from an ecophysiological model such as RATP. Based on several mock-ups with different LODs, it has been emphasized that three crown characteristics emerge as the most important characteristics to be measured or estimated: the PLA, the tree crown volume and the STAR. Indeed, these characteristics are strongly linked to the capacity of a tree crown to intercept light and, consequently, its transpiration rate. Among the mock-ups tested, the best result was obtained with a branching structure method that makes it possible to reconstruct the necessary characteristic values with high accuracy.

Even if envelope reconstruction methods obviously produce more approximate results, they allow us to obtain mock-ups in an easier and faster way than with the branching structure

method. In the perspective of simulating a realistic transpiration of a large diversity of urban trees, the LOD obtained with envelope reconstruction methods is relevant. A rapid and reliable method for retrieving the LAI and the LAD directly from TLS data should therefore be further developed to improve the simulated results. Although this study focuses on only one tree with specific geometry and foliage density for the moment, it should make it possible to highlight interesting reconstruction methods. It will be extended in the near future in order to focus on several trees with different geometries.

## **ACKNOWLEDGEMENTS**

The authors would like to thank the French National Research Agency (ANR) for funding the “COOLTREES” (ANR-17-CE22-0012-01) project. They would like also to thank the Atmo-IDEE project for the “INTERREG” program. They further wish to thank Yves Larnet, vice-president in charge of heritage at the University of Strasbourg, for granting us access to the “Palais Universitaire” garden, as well as the staff of the University of Strasbourg for their help. Finally, the authors would like to thank Samuel Guillemin and Jérôme Colin, members of the ICUBE laboratory, for their assistance with data acquisitions.

## References

- Béland, M., Baldocchi, D.D., Widlowski, J.-L., Fournier, R.A., Verstraete, M.M., 2014. On seeing the wood from the leaves and the role of voxel size in determining leaf area distribution of forests with terrestrial LiDAR. *Agricultural and Forest Meteorology* 184, 82-97.
- Béland, M., Widlowski, J.L., Fournier, R.A., Cote, J.F., Verstraete, M.M., 2011. Estimating leaf area distribution in savanna trees from terrestrial LiDAR measurements. *Agricultural and Forest Meteorology* 151, 1252-1266.
- Boudon, F., Preuksakarn, C., Ferraro, P., Diener, J., Nacry, P., Nikinmaa, E., Godin, C., 2014. Quantitative assessment of automatic reconstructions of branching systems obtained from laser scanning. *Annals of Botany* 114, 853-862.
- Bournez, E., Landes, T., Saudreau, M., Kastendeuch, P., Najjar, G., 2016. Impact of level of details in the 3d reconstruction of trees for microclimate modeling. *Int. Arch. Photogramm. Remote Sens. Spatial Inf. Sci. XLI-B8*, 257-264.
- Bournez, E., Landes, T., Saudreau, M., Kastendeuch, P., Najjar, G., 2017. From TLS point clouds to 3D models of trees: a comparison of existing algorithms for 3D tree reconstruction. *Int. Arch. Photogramm. Remote Sens. Spatial Inf. Sci. XLII-2/W3*, 113-120.
- Bowler, D.E., Buyung-Ali, L., Knight, T.M., Pullin, A.S., 2010. Urban greening to cool towns and cities: A systematic review of the empirical evidence. *Landscape and Urban Planning* 97, 147-155.
- Breda, N.J.J., 2003. Ground-based measurements of leaf area index: a review of methods, instruments and current controversies. *Journal of Experimental Botany* 54, 2403-2417.
- Caldwell, M.M., Meister, H.P., Tenhunen, J.D., Lange, O.L., 1986. Canopy structure, light microclimate and leaf gas exchange of *Quercus coccifera* L. in a Portuguese macchia: measurements in different canopy layers and simulations with a canopy model. *Trees-Structure and Function* 1, 25-41.
- Campbell, G.S., Norman, J.M., 1998. *An Introduction to Environmental Biophysics*, 2 ed. Springer-Verlag New York, p. 286.
- Chartier, P., 1966. Etude du microclimat lumineux dans la végétation. *Annales agronomiques* 17, 571-602.
- Clair-Maczulajtys, D., Bory, G., 1988. Modification de la répartition des glucides de réserve sous l'effet de l'élagage, chez deux arbres d'ornement (*Platanus acerifolia* Willd. et *Tilia platyphyllos* Scop.). *Bulletin de la Société Botanique de France. Actualités Botaniques* 135, 41-53.
- Da Silva, D., Balandier, P., Boudon, F., Marquier, A., Godin, C., 2012. Modeling of light transmission under heterogeneous forest canopy: an appraisal of the effect of the precision level of crown description. *Annals of Forest Science* 69, 181-193.
- Da Silva, D., Boudon, F., Godin, C., Sinoquet, H., 2008. Multiscale framework for modeling and analyzing light interception by trees. *Multiscale Modeling & Simulation* 7, 910-933.

Den Dulk, J.A., 1989. The interpretation of remote sensing, a feasibility study. PhD. Thesis, University of Wageningen, Wageningen.

Green, S.R., 1993. Radiation balance, transpiration and photosynthesis of an isolated tree. *Agricultural and Forest Meteorology* 64, 201-221.

IPCC, 2007. *Climate Change 2007: Synthesis Report. Contribution of Working Groups I, II and III to the Fourth Assessment Report of the Intergovernmental Panel on Climate Change: Core Writing Team, P., R.K and Reisinger, A. (eds.) (Ed.)*. IPCC, Geneva, Switzerland, p. 104.

Jarvis, P.G., 1976. The interpretation of the variations in leaf water potential and stomatal conductance found in canopies in the field. *Phil. Trans. Royal Society London B*. 273, 593 - 610.

Jiang, W., Xu, K., Cheng, Z.-Q., Martin, R.R., Dang, G., 2013. Curve skeleton extraction by coupled graph contraction and surface clustering. *Graphical Models* 75, 137-148.

Kong, F., Yan, W., Zheng, G., Yin, H., Cavan, G., Zhan, W., Zhang, N., Cheng, L., 2016. Retrieval of three-dimensional tree canopy and shade using terrestrial laser scanning (TLS) data to analyze the cooling effect of vegetation. *Agricultural and Forest Meteorology* 217, 22-34.

Kumakura, E., Nakaohkubo, K., Hoyano, A., 2010. Numerical Analysis of Solar Transmittance of a Deciduous Tree Crown. *Journal of The Japanese Institute of Landscape Architecture* 73, 573-576.

Landes, T., Hayot, C., Najjar, G., Kastendeuch, P., Saudreau, M., Colin, J., Luhache, R., Guillemain, S., 2014. Modélisation 3D d'arbre pour comprendre le climat urbain. *XYZ : revue de l'Association française de topographie* 141, 61-68.

Mei, J., Zhang, L., Wu, S., Wang, Z., Zhang, L., 2017. 3D tree modeling from incomplete point clouds via optimization and L1-MST. *International Journal of Geographical Information Science* 31, 999-1021.

Miller, J., Morgenroth, J., Gomez, C., 2015. 3D modelling of individual trees using a handheld camera: Accuracy of height, diameter and volume estimates. *Urban Forestry & Urban Greening* 14, 932-940.

Monsi, M., Saeki, T., 1953. Über den Lichtfaktor in den Pflanzengesellschaften und seine Bedeutung für die Stoffproduktion. *Japanese Journal of Botany* 14, 22-52.

Monteith, J.L., Unsworth, M.H., 1990. *Principles of environmental physics*. Edward Arnold, London.

Morgenroth, J., Gomez, C., 2014. Assessment of tree structure using a 3D image analysis technique—A proof of concept. *Urban Forestry & Urban Greening* 13, 198-203.

Mullaney, J., Lucke, T., Trueman, S.J., 2015. A review of benefits and challenges in growing street trees in paved urban environments. *Landscape and Urban Planning* 134, 157-166.

Najjar, G., Colin, J., Kastendeuch, P., Ngao, J., Saudreau, M., Landes, T., Ameglio, T., Luhache, R., Guillemain, S., 2015. A three years long fieldwork experiment to monitor the role of

vegetation on the urban climate of the city of Strasbourg, France, 9th International Conference on Urban Climate. International Association for Urban Climate., Toulouse, FRA.

Nilson, T., 1971. A theoretical analysis of the frequency of gaps in plant stands. *Agricultural Meteorology* 8, 25-38.

Noilhan, J., Planton, S., 1989. A simple parameterization of land surface processes for meteorological models. *Monthly Weather Review* 117, 536-549.

Oke, T.R., 1982. The energetic basis of the urban heat island. *Quarterly Journal of the Royal Meteorological Society* 108, 1-24.

Oshio, H., Asawa, T., Hoyano, A., Miyasaka, S., 2015. Estimation of the leaf area density distribution of individual trees using high-resolution and multi-return airborne LiDAR data. *Remote Sensing of Environment* 166, 116-125.

Peters, E.B., Hiller, R.V., McFadden, J.P., 2011. Seasonal contributions of vegetation types to suburban evapotranspiration. *Journal of Geophysical Research: Biogeosciences* 116.

Phattaralerphong, J., Sinoquet, H., 2005. A method for 3D reconstruction of tree crown volume from photographs: assessment with 3D-digitized plants. *Tree Physiology* 25, 1229-1242.

Redon, E.C., Lemonsu, A., Masson, V., Morille, B., Musy, M., 2017. Implementation of street trees within the solar radiative exchange parameterization of TEB in SURFEX v8.0. *Geoscientific Model Development* 10, 385-411.

Rosenzweig, C., Solecki, W.D., Parshall, L., Lynn, B., Cox, J., Goldberg, R., Hodges, S., Gaffin, S., Slosberg, R.B., Savio, P., Dunstan, F., Watson, M., 2009. Mitigating new york city's heat island Integrating Stakeholder Perspectives and Scientific Evaluation. *Bulletin of the American Meteorological Society* 90, 1297-1312.

Ross, J., 1981. *The Radiation Regime and Architecture of Plant Stands*. Junk W. Pubs, The Hague.

Saudreau, M., Pincebourde, S., Dassot, M., Adam, B., Loxdale, H.D., Biron, D.G., 2013. On the canopy structure manipulation to buffer climate change effects on insect herbivore development. *Trees-Structure and Function* 27, 239-248.

Sellier, D., Fourcaud, T., 2005. A mechanical analysis of the relationship between free oscillations of *Pinus pinaster* Ait. saplings and their aerial architecture. *Journal of Experimental Botany* 56, 1563-1573.

Sinoquet, H., Le Roux, X., Adam, B., Ameglio, T., Daudet, F.A., 2001. RATP: a model for simulating the spatial distribution of radiation absorption, transpiration and photosynthesis within canopies: application to an isolated tree crown. *Plant Cell and Environment* 24, 395-406.

Sinoquet, H., Rivet, P., 1997. Measurement and visualization of the architecture of an adult tree based on a three-dimensional digitising device. *Trees-Structure and Function* 11, 265-270.

Sinoquet, H., Sonohat, G., Phattaralerphong, J., Godin, C., 2005. Foliage randomness and light interception in 3-D digitized trees: an analysis from multiscale discretization of the canopy. *Plant Cell and Environment* 28, 1158-1170.

Sinoquet, H., Stephan, J., Sonohat, G., Lauri, P.E., Monney, P., 2007. Simple equations to estimate light interception by isolated trees from canopy structure features: assessment with three-dimensional digitized apple trees. *New Phytologist* 175, 94-106.

Sonohat, G., Sinoquet, H., Kulandaivelu, V., Combes, D., Lescourret, F., 2006. Three-dimensional reconstruction of partially 3D-digitized peach tree canopies. *Tree Physiology* 26, 337-351.

van Leeuwen, M., Nieuwenhuis, M., 2010. Retrieval of forest structural parameters using LiDAR remote sensing. *European Journal of Forest Research* 129, 749-770.

Wang, Y.P., Jarvis, P.G., 1990. Description and validation of an array model - maestro. *Agricultural and Forest Meteorology* 51, 257-280.

Xu, H., Gossett, N., Chen, B.Q., 2007. Knowledge and heuristic-based modeling of laser-scanned trees. *Acm Transactions on Graphics* 26, 1-19.

Zhu, C., Zhang, X.P., Hu, B.G., Jaeger, M., 2008. Reconstruction of tree crown shape from scanned data, in: Pan, Z.G., Zhang, X.P., ElRhalibi, A., Woo, W., Li, Y. (Eds.), *Technologies for E-Learning and Digital Entertainment, Proceedings*, pp. 745-756.

## Figures and table legends

**Fig. 1.** The silver linden tree under study a) with leaves and without leaves and b) the field TLS acquisition, with at least four stations around the trees, in order to obtain c) tree point clouds. The point cloud used for the 3D reconstruction of the tree with leaves contains about 92 000 points, and this one without leaves is composed of about 756 000 points.

**Fig. 2.** Mock-ups reconstructed according to three groups of reconstruction methods, followed by methods used for leaf distribution. Group I contains seven mock-ups with a high LOD, decreasing from the reference ( $\text{LOD}_{\text{ref}(I)}$ ) to  $\text{LOD}_{1(I)}$ . All mock-ups were reconstructed based on different branching structure reconstruction methods and on **(A)** shoot allometry for leaf distribution around shoots. They therefore have different TLA values, except for  $\text{LOD}_{4\text{-TLAref}(I)}$ ,  $\text{LOD}_{2\text{-TLAref}(I)}$  and  $\text{LOD}_{1\text{-TLAref}(I)}$ , which have a TLA equal to  $\text{LOD}_{\text{ref}(I)}$ . Group II, using envelope reconstruction methods, is composed of four mock-ups with an LOD that is coarser than in Group I, decreasing from  $\text{LOD}_{0.8(II)}$  to  $\text{LOD}_{0(II)}$ . A uniform leaf distribution in short head envelopes **(B)** and in crown envelopes **(C)**, respectively, is used to reconstruct  $\text{LOD}_{0.8(II)}$  and the other LODs of Group II. Group III, using voxel reconstruction methods and **(D)** uniform leaf distribution in each voxel, contains the four mock-ups that have the lowest LOD, from  $\text{LOD}_{0.5\text{-Vox}20(III)}$  to  $\text{LOD}_{0\text{-Vox}50(III)}$ .

**Fig. 3.** Comparison of tree crown characteristics, i.e., Volume ( $\text{m}^3$ ), Projected Leaf Area (PLA) ( $\text{m}^2$ ), Leaf Area Index (LAI), Leaf Area Density (meanLAD) ( $\text{m}^2/\text{m}^3$ ), clumping factor ( $\mu$ ) and Silhouette-to-Total Area Ratio (STAR), between the three groups of tree reconstruction methods. These results were obtained on the basis of an analysis of variance and a Fisher's LSD test. For each group, the same number of mock-ups was used, i.e.,  $n = 4$ .  $\text{LOD}_{4\text{-TLAref}(I)}$ ,

LOD 2-TLAref<sub>(1)</sub> and LOD 1-TLAref<sub>(1)</sub> were not used for this analysis. The letters a, b and ab indicate the significance of homogeneous groups with the p-value level set to 0.05.

**Fig. 4.** Comparison of the cooling performances of the tree mock-ups compared to the reference case, i.e., LOD ref<sub>(1)</sub>. Only the mean linear regressions obtained per group of reconstruction methods, i.e., Group I, II and III, are shown. The slopes,  $a_T$ , of the linear regression curves obtained for each mock-up and each group are listed in Table 1.

**Fig. 5.** Comparison of the  $a_T$  slope, obtained for each mock-up by comparing their deviation of the simulated transpiration rate with respect to the reference, and the Projected Leaf Area (PLA) characteristic deduced from each mock-up. On the basis of the mock-ups, the three reconstruction groups can be distinguished by three different symbols. The characteristics of the regression line (red line), i.e., the coefficient of determination  $R^2$ , the slope  $a$  and the intercept  $b$ , presented in this figure are also reported in Table 2.

**Fig. 6.** Comparison of the  $a_T$  slope, obtained for each mock-up their deviation the simulated transpiration rate with respect to the reference, and the light interception ability estimated with the diffuse Silhouette-to-Total Area Ratio (STAR) characteristic deduced from each mock-up. On the basis of the mock-ups, the three reconstruction groups can be distinguished by three different symbols. The characteristics of the regression line (red line), i.e., the coefficient of determination  $R^2$ , the slope  $a$  and the intercept  $b$ , presented in this figure are also reported in Table 2.

**Figures:**

**Fig. 1.**

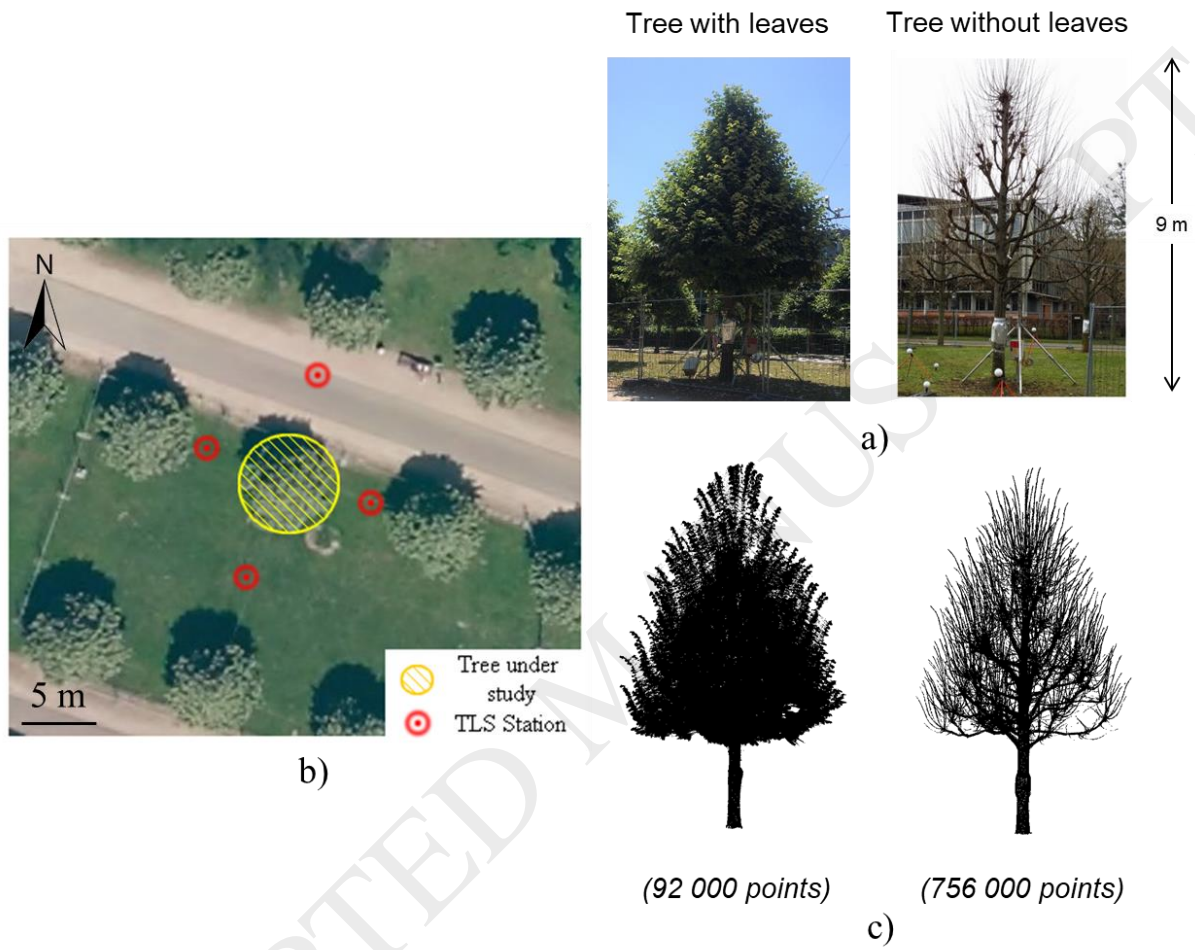
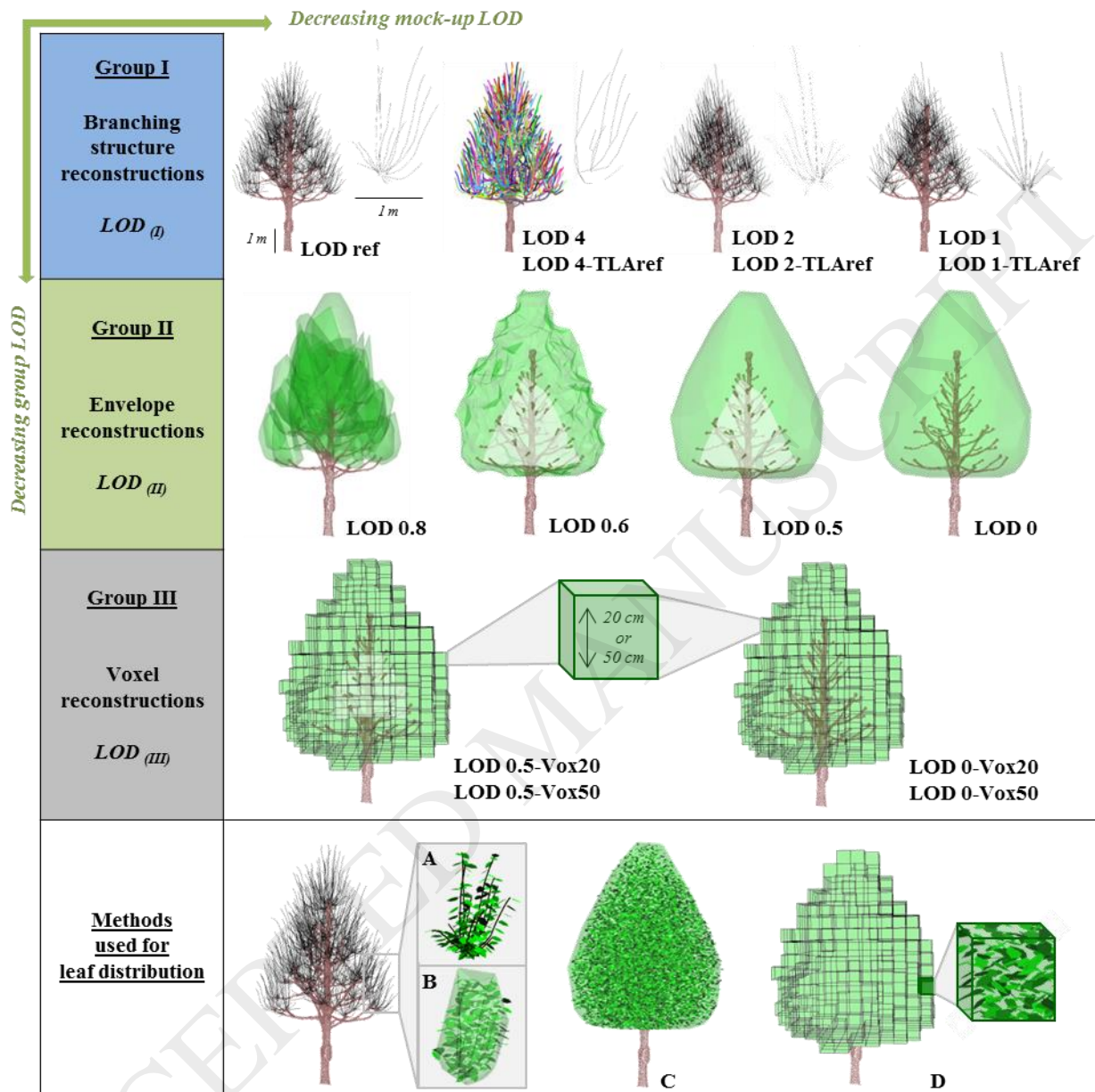
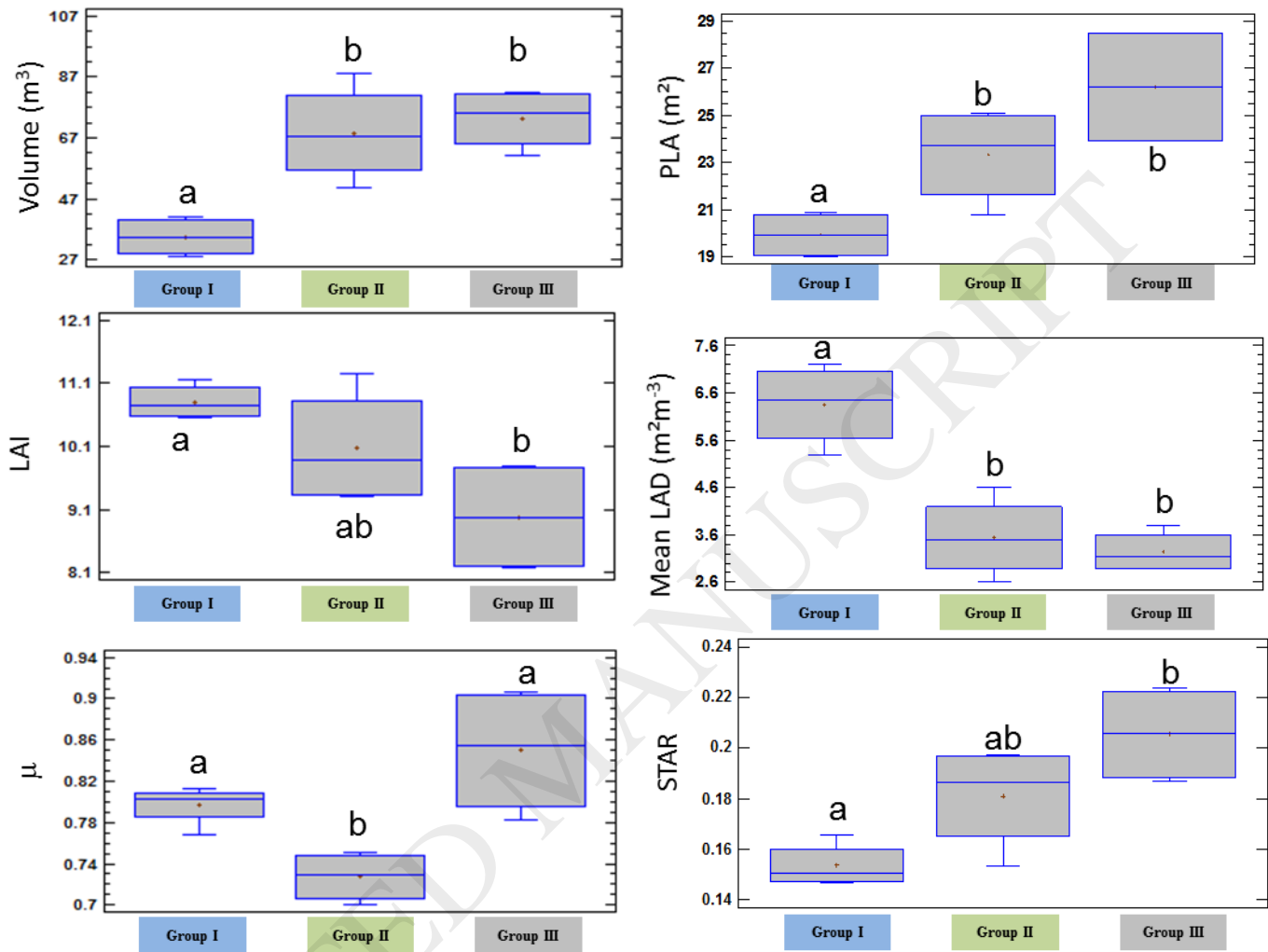


Fig. 2.



**Fig. 3.**

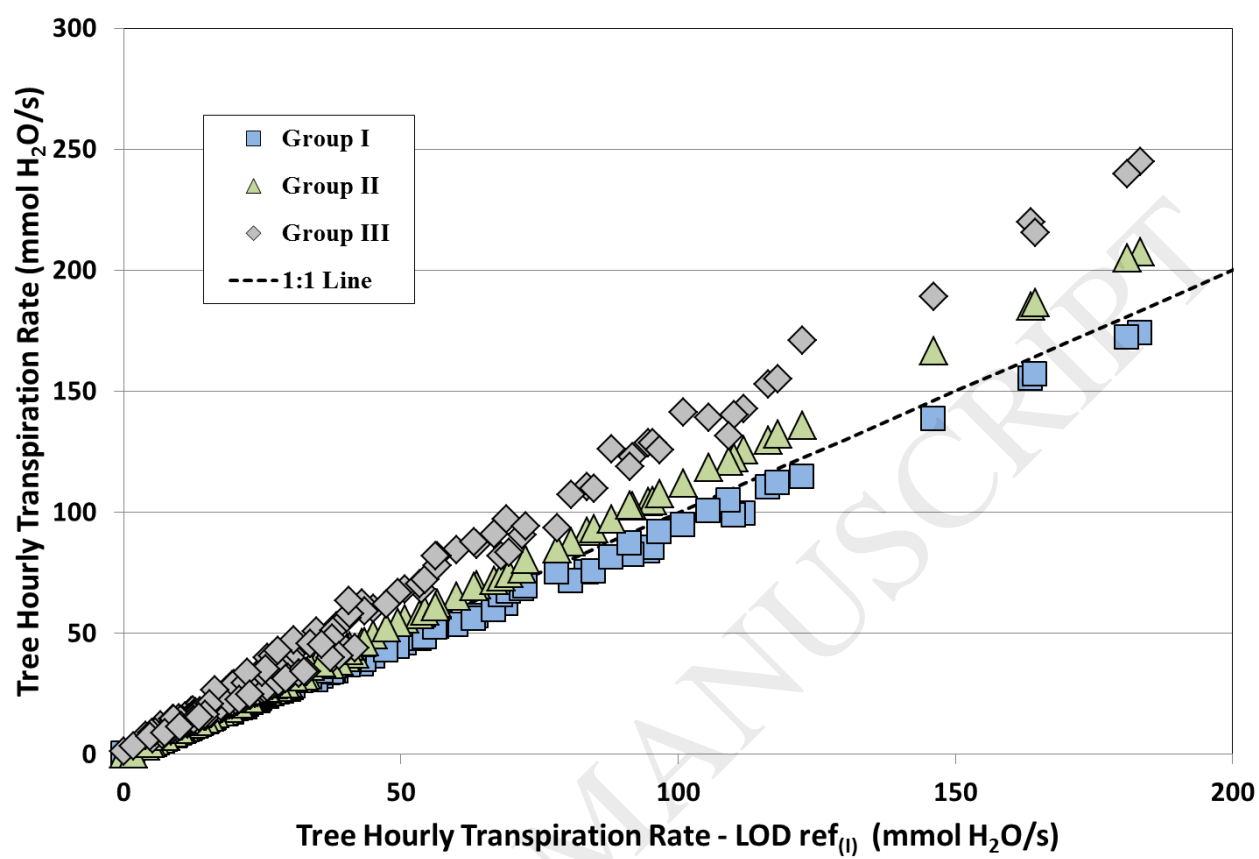
**Fig. 4.**

Fig. 5.

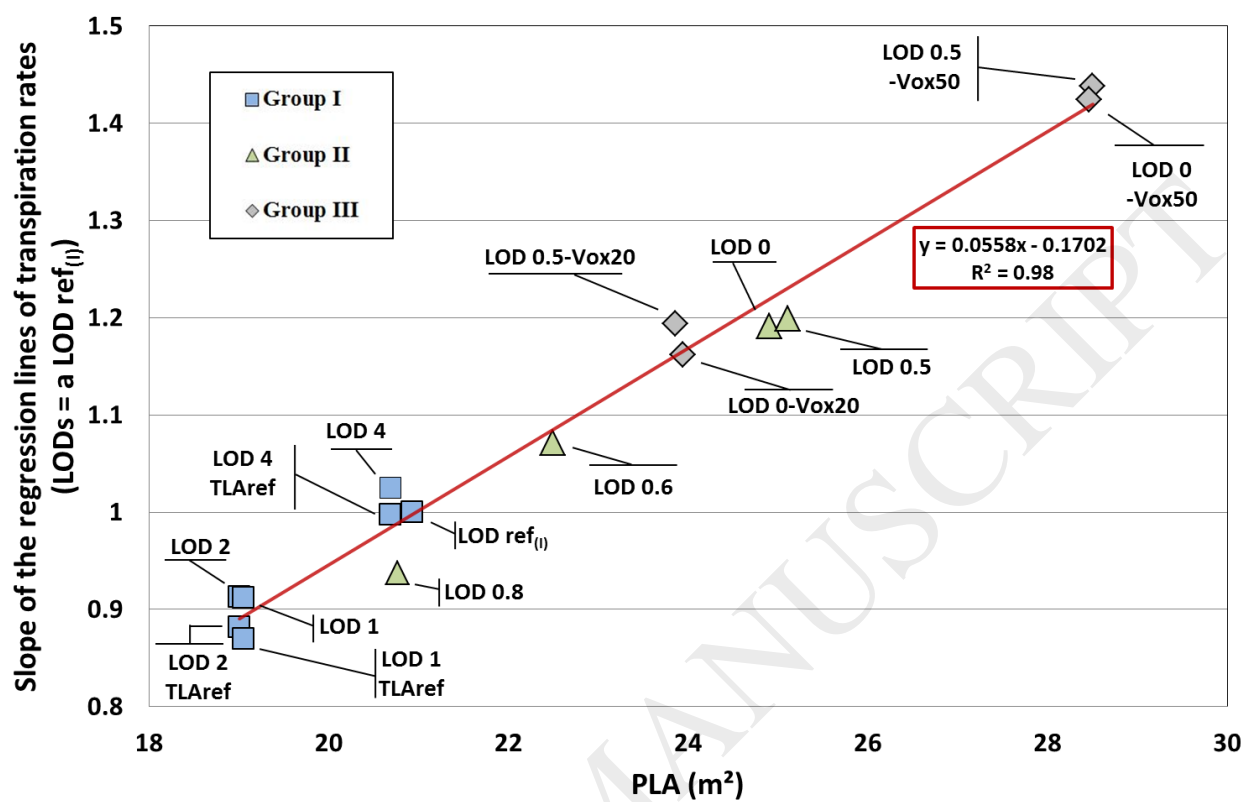
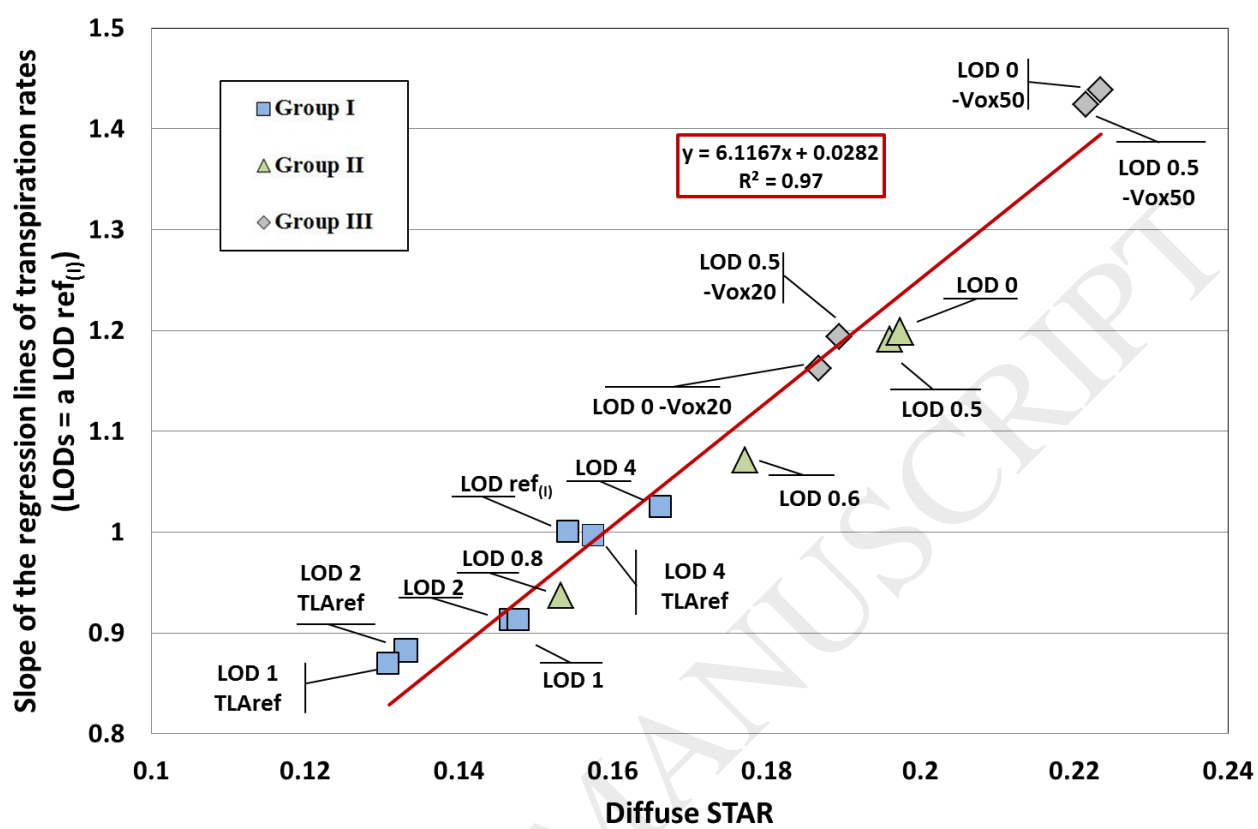


Fig. 6.



**Tables:****Table 1**

The metrics, light and physiology characteristics of the 15 mock-ups according to the reconstruction method used. The primary metric characteristics, i.e., the Total Leaf Area (TLA), the volume and the Projected Leaf Area (PLA), make it possible to compute the other metric characteristics such as the mean Leaf Area Density (meanLAD) and the Leaf Area Index (LAI). The clumping factor ( $m$ ) and the diffuse Silhouette-to-Total Area Ratio (STAR) are linked to the tree foliage and the light interception in the crown. The physiology characteristics are obtained with the linear regression between the transpiration rates of all the mock-ups compared to the transpiration simulated with the reference mock-up. The slope,  $a_r$ , of these linear regressions and the percentages of transpiration deviation with respect to the reference mock-up are depicted in the two last rows of this table. Values are given per mock-up and per reconstruction group.

|                |   | Group I - Branching Structure |       |       |       |                 |                 |                 | Group II - Envelope |         |         |       | Group III - Voxels |                 |                   |                 |
|----------------|---|-------------------------------|-------|-------|-------|-----------------|-----------------|-----------------|---------------------|---------|---------|-------|--------------------|-----------------|-------------------|-----------------|
|                | Characteristics                           | LOD <sub>ref(t)</sub>         | LOD 4 | LOD 2 | LOD 1 | LOD 4<br>TLAref | LOD 2<br>TLAref | LOD 1<br>TLAref | LOD 0.8             | LOD 0.6 | LOD 0.5 | LOD 0 | LOD 0.5-<br>Vox50  | LOD 0-<br>Vox50 | LOD 0.5-<br>Vox20 | LOD 0-<br>Vox20 |
| <b>Metrics</b> | Total Leaf Area (m <sup>2</sup> )         | 233.6                         | 218.8 | 207.1 | 201.2 | 233.6           | 233.6           | 233.6           | 233.4               | 233.4   | 233.4   | 233.4 | 233.4              | 233.4           | 233.4             | 233.4           |
|                | Volume (m <sup>3</sup> )                  | 38.8                          | 41.0  | 30.0  | 28.0  | 41.0            | 30.0            | 28.0            | 50.8                | 61.7    | 73.2    | 88.2  | 81.3               | 81.9            | 61.2              | 69.0            |
|                | meanLAD (m <sup>2</sup> /m <sup>3</sup> ) | 6.0                           | 5.3   | 6.9   | 7.2   | 5.7             | 7.8             | 8.4             | 4.6                 | 3.8     | 3.2     | 2.6   | 2.9                | 2.9             | 3.8               | 3.4             |

|                   |  |          |        |        |        |        |        |        |        |        |        |        |        |        |        |        |
|-------------------|--|----------|--------|--------|--------|--------|--------|--------|--------|--------|--------|--------|--------|--------|--------|--------|
|                   | PLA (m <sup>2</sup> )  | 20.9     | 20.7   | 19.0   | 19.1   | 20.7   | 19.0   | 19.1   | 20.8   | 22.5   | 24.9   | 25.1   | 28.5   | 28.5   | 23.9   | 23.9   |
|                   | LAI (m <sup>2</sup> /m <sup>2</sup> )                        | 11.2     | 10.6   | 10.9   | 10.6   | 11.3   | 12.3   | 12.3   | 11.2   | 10.4   | 9.4    | 9.3    | 8.2    | 8.2    | 9.8    | 9.8    |
| <b>Light</b>      | $\mu$ (Clumping factor)                                      | 0.802    | 0.769  | 0.804  | 0.813  | 0.754  | 0.797  | 0.797  | 0.701  | 0.711  | 0.747  | 0.750  | 0.906  | 0.902  | 0.807  | 0.783  |
|                   | Diffuse STAR   | 0.154    | 0.166  | 0.147  | 0.148  | 0.157  | 0.133  | 0.131  | 0.153  | 0.177  | 0.196  | 0.197  | 0.223  | 0.222  | 0.190  | 0.187  |
| <b>Physiology</b> | ar: Slope Transpiration Rate LODs vs. LOD ref <sub>(1)</sub> | 1.0000   | 1.0248 | 0.9123 | 0.9120 | 0.9969 | 0.8815 | 0.8693 | 0.9373 | 1.0715 | 1.1910 | 1.1987 | 1.4385 | 1.4244 | 1.1941 | 1.1623 |
|                   | Deviation from the LOD ref <sub>(1)</sub> case               | By LOD   | +2%    | -9%    | -9%    | 0%     | -12%   | -13%   | -6%    | +7%    | +19%   | +20%   | +44%   | +42%   | +19%   | +16%   |
|                   |  | By group | -7%    |        |        |        |        |        | +10%   |        |        | +30%   |        |        |        |        |

**Table 2**

Multiple regression analysis between the slopes,  $a_T$ , representing the deviation of the simulated transpiration rates between all the mock-ups and the reference case and tree crown characteristics such as the Projected Leaf Area (PLA), the Silhouette-to-Total Area Ratio (STAR), the Leaf Area Index (LAI), the Volume, the Leaf Area Density (meanLAD) and the clumping factor ( $m$ ). This analysis leads us to compute six statistical indices: the Mean Square Error (MSE), the Mean Average Error (MAE), the coefficient of determination ( $R^2$ ), the Mallows' coefficient ( $C_p$ ), the slope of the regression ( $a$ ) and the intercept of the regression ( $b$ ). The significance of each simple linear regression was assessed with an F-test with a significant p-value level set to 0.05.

| <b>Characteristics</b>  | <b>MSE</b> | <b>MAE</b> | <b>R<sup>2</sup></b> | <b>C<sub>p</sub></b> | <b>a</b> | <b>b</b> |
|-------------------------|------------|------------|----------------------|----------------------|----------|----------|
| <b>PLA</b>              | 0.0007     | 0.0211     | 97.9991              | 1191.46              | 0.0558   | -0.1702  |
| <b>STAR</b>             | 0.0011     | 0.0273     | 97.0533              | 1759.81              | 6.1167   | 0.0282   |
| <b>LAI</b>              | 0.0037     | 0.0451     | 89.7655              | 6139.43              | -0.1380  | 2.5094   |
| <b>Volume</b>           | 0.0069     | 0.0602     | 81.0536              | 11374.90             | 0.0077   | 0.6699   |
| <b>meanLAD</b>          | 0.0093     | 0.0656     | 74.2273              | 15477.20             | -0.0813  | 1.4847   |
| <b><math>\mu</math></b> | 0.0257     | 0.1312     | 28.9902              | 42662.50             | 1.7093   | -0.2685  |